Inorganic Chemistry

Article

pubs.acs.org/IC

Synthesis, Crystal Structure, and High Temperature Transport Properties of *p*-Type $Cu_2Zn_{1-x}Fe_xSnSe_4$

Yongkwan Dong,[†] Hsin Wang,[‡] and George S. Nolas*[,†]

[†]Department of Physics, University of South Florida, Tampa, Florida 33620, United States

[‡]Materials Science and Technology Division, Oak Ridge National Laboratory, Oak Ridge, Tennessee 37831, United States

Supporting Information

ABSTRACT: Iron substituted $Cu_2Zn_{1-x}Fe_xSnSe_4$ stannites were synthesized by reaction of the constituent elements and subsequent annealing, followed by densification by hot-pressing. The compositions for each specimen were confirmed with a combination of Rietveld refinement and elemental analysis. Refinement results indicated that only the 2*a* site was occupied by Zn and Fe. High temperature transport properties were measured from 300 to 800 K. The electrical resistivity and thermal conductivity decrease with increasing Fe content. For the lower Fe content specimens with $x = 0.2$ and 0.4, the electrical properties are strongly temperature dependent, unlike that of the higher Fe content specimens ($x = 0.6$ and 0.8). A maximum ZT value of 0.46 was obtained at 800 K for $Cu_2Zn_{0.4}Fe_{0.6}SnSe_4$.

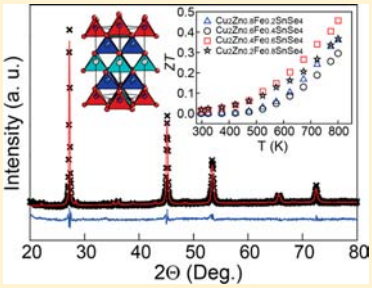

INTRODUCTION

Thermoelectric devices can directly convert heat to electrical energy. Good thermoelectric materials require a low electrical resistivity, ρ, to lessen Joule heating, a low thermal conductivity, κ, to reduce thermal losses, and a large absolute Seebeck coefficient, S, to obtain high thermoelectric performance as defined by the dimensionless thermoelectric figure-of-merit ($ZT = S^2T/\rho\kappa$, where T is the absolute temperature) in the temperature range of interest. The three material properties that define ZT can be varied by doping; however, they are not independent of each other.[1−4]

Beyond simple or modified chalcogenides such as Bi_2Te_3, PbTe, and TAGS ($AgGeTe_2$−GeTe), recently Cu-based chalcogenides[5−14] and oxychalcogenides[15−17] have attracted attention as thermoelectric materials because of low κ values attributed to their crystal structures. Although these materials possess relatively wide band gaps, a property that is typically not of interest for thermoelectric applications,[4] the electrical properties can be modified by appropriate doping and/or variations in stoichiometry. Among them, Sn containing compositions with the stannite structure type, such as $Cu_2CdSnSe_4$[9] and $Cu_2ZnSnSe_4$,[10,11] have been shown to possess good thermoelectric properties. In addition, most compositions are made of Earth-abundant and nontoxic materials. These materials have also been synthesized in nanocrystalline form in order to investigate nanoscale effects on the thermoelectric properties.[18−20]

It has been reported that the lattice thermal conductivity, κ_L, of the $Cu_2Zn_{1-x}Fe_xGeSe_4$ compositions[12] can be greatly reduced, as compared to $Cu_2ZnGeSe_4$, by point defect scattering from restructuring of the cations. These compositions have been reported to possess crystal structures between that of stannites (for example, $Cu_2ZnGeSe_4$ with centrosymmetric tetragonal space group $I\bar{4}2m$) and kesterites (for example, $Cu_2FeGeSe_4$ with noncentrosymmetric $I\bar{4}$).[12] However, the synthesis, crystal structure, and transport properties of Fe substituted $Cu_2ZnSnSe_4$ with the tetragonal stannite crystal structure have not been reported, to our knowledge. In this paper, we report on the synthesis, crystal structure, and high temperature transport properties of solid solution stannites $Cu_2Zn_{1-x}Fe_xSnSe_4$ with $0.2 \leq x \leq 0.8$ and compare our results to those of $Cu_2ZnSnSe_4$.[11]

EXPERIMENTAL SECTION

Synthesis. All compounds were prepared by direct reaction of the high purity elements. Cu powder (99.9%, Alfa Aesar), Fe powder (99.998%, Alfa Aesar), Zn shot (99.9999%, Alfa Aesar), Sn powder (99.999%, Alfa Aesar), and Se powder (99.999%, Alfa Aesar) were loaded into silica ampules in stoichiometric ratios $Cu_2Zn_{1-x}Fe_xSnSe_4$ (where $x = 0.2$, 0.4, 0.6, and 0.8). The reaction ampules were sealed in quartz tubes, heated to 973 K, and subsequently held at this temperature for 5 days. The furnace was turned off, and the reaction tubes were quenched to room temperature in the air. The products were then ground into fine powders, cold pressed into pellets, and annealed at 973 K for one week. Additional grinding and annealing were performed in order to further promote homogeneity of the products. After appropriate annealing, the products were ground into fine powders and sieved (325 mesh) inside a glovebox, then loaded into graphite dies for hot pressing. Densification was accomplished by hot pressing at 873 K and 150 MPa for 3 h under a N_2 flow. The density of the hot-pressed pellets was determined by measurement of their dimensions and weight after polishing the surfaces of the pellets. These measurements indicated that high density polycrystalline specimens (>96% of theoretical density) were obtained.

Physical Characterization. X-ray diffraction (XRD) and electron probe analyses were used to examine the purity and chemical composition of the specimens. Powder XRD data were collected with a

Received: September 27, 2013
Published: November 27, 2013

   dx.doi.org/10.1021/ic402455x | Inorg. Chem. 2013, 52, 14364−14367

Table 1. Rietveld Refinement[a] Results for $Cu_2Zn_{1-x}Fe_xSnSe_4$

nominal x	0.2	0.4	0.6	0.8
composition	$Cu_2Zn_{0.8(1)}Fe_{0.2(1)}Sn_{1.0(1)}Se_{4.0(1)}$	$Cu_2Zn_{0.6(1)}Fe_{0.4(1)}Sn_{1.0(1)}Se_{4.0(1)}$	$Cu_2Zn_{0.4(1)}Fe_{0.6(1)}Sn_{1.0(1)}Se_{4.0(1)}$	$Cu_2Zn_{0.2(1)}Fe_{0.7(1)}Sn_{1.1(1)}Se_{4.0(1)}$
space group, Z	$I\bar{4}2m$ (No. 121), 2			
a, Å	5.695 (1)	5.694 (2)	5.682 (2)	5.693 (1)
c, Å	11.387 (5)	11.379 (8)	11.375 (8)	11.331 (2)
c/a	1.999	1.998	2.002	1.990
V, Å^3	369.3 (1)	368.9 (1)	367.2 (1)	367.2 (1)
radiation	graphite monochromated Cu K_α (1.54056 Å)			
D_{calcd}, g/cm^3	5.621	5.608	5.619	5.601
reduced χ^2	3.073	2.860	6.155	3.451
wR_p, R_p	0.0841, 0.0636	0.0799, 0.0594	0.0780, 0.0533	0.0571, 0.0425
Cu−Se, Å	2.4236 (5)	2.4226 (8)	2.4183 (8)	2.4187 (2)
Zn/Fe−Se, Å	2.4541 (5)	2.4545 (9)	2.4506 (9)	2.4529 (2)
Sn−Se, Å	2.5678 (5)	2.5655 (9)	2.5629 (9)	2.5599 (2)

[a]Atomic positions: Cu, 4d (0,0.5,0.25); Zn/Fe, 2a (0,0,0); Sn, 2b (0,0,0.5); Se, 8i (x,x,z).

Bruker D8 Focus diffractometer in Bragg−Brentano geometry using Cu $K_{\alpha,\beta}$ radiation and a graphite monochromator and examined by the Rietveld method using the GSAS suite of programs.[21] Energy dispersive X-ray analysis (EDX) of the hot-pressed pellets was accomplished with an Oxford INCA X-Sight 7582 M equipped scanning electron microscope (JEOL JSM-6390LV). The average atomic ratios were calculated from at least 12 data sets obtained from random positions of the hot pressed pellet for each specimen.

High temperature S and ρ were measured on parallelepipeds, cut from the hot pressed pellets, with an ULVAC ZEM-3 system (experimental uncertainty of 5−8% for S and ρ at elevated temperatures). High temperature κ values were determined using the equation $\kappa = D{\cdot}\alpha{\cdot}C_p$ where D is the measured density from geometry, α is the measured thermal diffusivity, and C_p is the specific heat. Thermal diffusivity measurements employed the laser flash method in a flowing He environment with a NETZSCH LFA 457 system. The uncertainty in the thermal diffusivity measurements was ~5%. Heat capacity C_p ($\approx C_v$) was estimated with the Dulong-Petit limit ($C_v = 3nR$, where n is the number of atoms per formula unit and R is the ideal gas constant). At high temperatures, this may sometimes result in an underestimation of C_p, thus affecting κ; however it is a relatively good method for comparing the effect of doping and compositional changes since it eliminates the uncertainties associated with C_p measurements.[22]

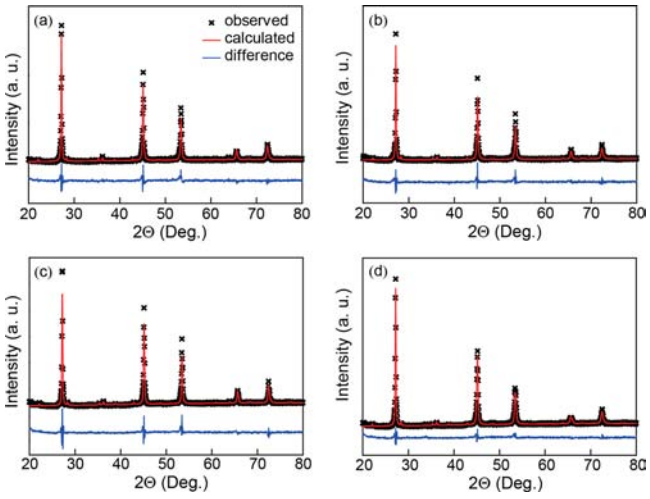

Figure 1. Powder XRD data for (a) $Cu_2Zn_{0.8}Fe_{0.2}SnSe_4$, (b) $Cu_2Zn_{0.6}Fe_{0.4}SnSe_4$, (c) $Cu_2Zn_{0.4}Fe_{0.6}SnSe_4$, and (d) $Cu_2Zn_{0.2}Fe_{0.8}SnSe_4$ including profile fit, profile difference, and profile residuals from Rietveld refinement.

RESULTS AND DISCUSSION

Structural Characterization. Powder XRD revealed the formation of single-phase $Cu_2Zn_{1-x}Fe_xSnSe_4$ solid solutions. The powder XRD patterns for each specimen were found to correspond to the tetragonal stannite structure. The lattice parameters for this tetragonal structure were first estimated and then refined. The initial positional parameters for all the atoms in the structure were from data on $Cu_2ZnSnSe_4$[23] and $Cu_2FeSnSe_4$.[24] For all specimens, the space group $I\bar{4}2m$ (No. 121) was applied to refine the crystal structure. Detailed refinement results are shown in Table 1. The observed and calculated XRD patterns and the difference profiles for each specimen are given in Figure 1.

A structural change, from stannite to kesterite, with cationic arrangement in the crystal structure has been reported for $Cu_2Zn_{1-x}Fe_xSnS_4$[25,26] and $Cu_2Zn_{1-x}Fe_xGeSe_4$[12] solid solutions. These reports show that Fe replaces Zn on the 2a crystallographic site while Cu resides on the 4d crystallographic site for low Fe concentrations. For the higher Fe content compositions, Cu also occupies the 2a site with Zn and Fe, and the residual Zn is located on the 4d site. Eventually, for the highest Fe content compositions, the 2a site is occupied by Cu, and Cu and Fe occupy the 4d site. For $Cu_2Cd_{1-x}Mn_xSnSe_4$[27] and $Cu_2Cd_{1-x}Fe_xSnSe_4$[28] solid solutions, it was reported that Cd replaced Mn[27] or Fe[28] on the 2a site because both end compositions form in the stannite structure type. Both models were applied for each of the specimens in this study in order to determine the cationic configuration, and our analyses indicated that the $Cu_2Cd_{1-x}M_xSnSe_4$ (M = Mn and Fe) model is more reasonable for these compositions. This is not surprising since both end compositions, $Cu_2ZnSnSe_4$[23] and $Cu_2FeSnSe_4$,[24] possess the same tetragonal stannite structure type, similar to the case for the $Cu_2Cd_{1-x}M_xSnSe_4$ (M = Mn, Fe) solid solutions.[27,28] Figure 2 shows the crystal structure of our $Cu_2Zn_{1-x}Fe_xSnSe_4$ solid solutions based on our refinement results. Each metal atom is surrounded by four Se atoms in a tetrahedral geometry. Each Se atom is also tetrahedrally bounded by four metal atoms. Metal−Se bond distances range from 2.4183(8) Å to 2.4236(9) Å for Cu, 2.4506(9) Å to 2.4545 (9) Å for Zn/Fe, and 2.5599 (2) Å to 2.5678 (5) Å for Sn. For all specimens, there are no significant differences of the Cu−Se, Zn/Fe−Se, and Sn−Se bond distances shown in Table 1. These values are in good agreement with those found in other related compounds with the same structure type.[23,24,27,28]

dx.doi.org/10.1021/ic402455x | Inorg. Chem. 2013, 52, 14364−14367

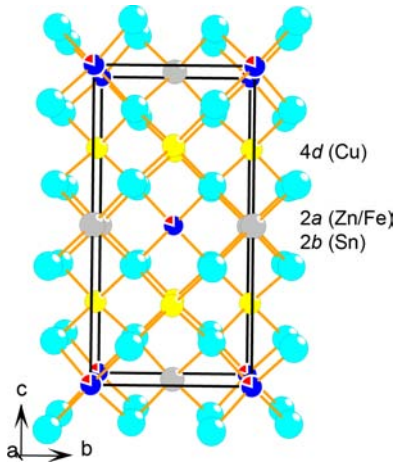

Figure 2. The crystal structure of $Cu_2Zn_{0.2}Fe_{0.8}SnSe_4$ along the crystallographic *a* axis. Cu atoms are yellow, Zn atoms are red, Fe atoms are blue, Sn atoms are gray, and Se atoms are cyan.

Transport Properties. Figure 3 shows temperature dependent ρ and S values from 300 to 800 K. All specimens exhibit relatively high ρ at room temperature, as expected for relatively wide band gap semiconductors.[12,20] For the high Fe content compositions, $Cu_2Zn_{0.4}Fe_{0.6}SnSe_4$ and $Cu_{2.2}Zn_{0.2}Fe_{0.8}SnSe_4$, the ρ values are significantly lower than that of the two compositions with a lower Fe content. As shown in Figure 3, the ρ values for $Cu_2Zn_{0.8}Fe_{0.2}SnSe_4$ and $Cu_2Zn_{0.6}Fe_{0.4}SnSe_4$ are strongly temperature dependent and decrease rapidly with increasing temperature, while those for $Cu_2Zn_{0.4}Fe_{0.6}SnSe_4$ and $Cu_2Zn_{0.2}Fe_{0.8}SnSe_4$ are much less temperature dependent. In addition, the ρ values decrease with increasing Fe content, with an approximately 2 orders of magnitude difference in ρ between $Cu_2Zn_{0.8}Fe_{0.2}SnSe_4$ and $Cu_2Zn_{0.2}Fe_{0.8}SnSe_4$ at room temperature. All specimens exhibit positive S values, as expected for these p-type materials. For $Cu_2Zn_{0.8}Fe_{0.2}SnSe_4$ and $Cu_2Zn_{0.6}Fe_{0.4}SnSe_4$, the S values increase with increasing temperature and reach a maximum at 500 K, corresponding to the change of the slope in ρ. This reduction in S at high temperatures is presumably due to thermal excitation of minority carriers. According to Goldsmid and Sharp,[29] $S_{max} \approx E_g/2eT_{max}$ where E_g is the energy gap, e is the elementary charge, and T_{max} is the absolute temperature at S_{max}. Employing this formulation, E_g values of 0.38 and 0.33 eV for $Cu_2Zn_{0.8}Fe_{0.2}SnSe_4$ and $Cu_2Zn_{0.6}Fe_{0.4}SnSe_4$, respectively, are obtained at 500 K. For $Cu_2Zn_{0.4}Fe_{0.6}SnSe_4$, the S values increase very slowly with temperature up to the maximum measured temperature. The S values for $Cu_2Zn_{0.2}Fe_{0.8}SnSe_4$ show a slightly different behavior, displaying relatively little temperature dependence up to 700 K, then decrease with increasing temperature. This is also likely due to the thermal excitation of minority carriers.

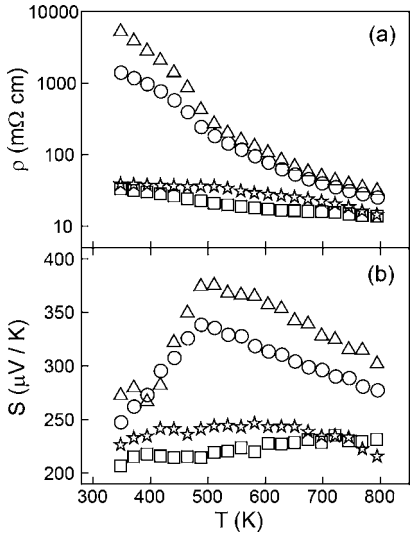

Figure 3. Temperature dependent (a) ρ and (b) S data for $Cu_2Zn_{0.8}Fe_{0.2}SnSe_4$ (△), $Cu_2Zn_{0.6}Fe_{0.4}SnSe_4$ (○), $Cu_2Zn_{0.4}Fe_{0.6}SnSe_4$ (□), $Cu_2Zn_{0.2}Fe_{0.8}SnSe_4$ (☆).

High temperature κ values are shown in Figure 4a. The κ values decrease rapidly with increasing temperature, and with increasing Fe content. The κ_L values (Figure 4b) were estimated using the Wiedemann–Franz relation $\kappa = \kappa_E + \kappa_L$, where $\kappa_E = L_0\sigma T$, σ is the electrical conductivity, and $L_0 = 2.0 \times 10^{-8}$ V^2/K^2, the Lorenz number.[9,11] At lower temperatures, κ_L is the dominant contribution ($\kappa \sim \kappa_L$) in these specimens due to the relatively high ρ values for all specimens. However, at higher temperatures, κ_E is larger due to the fact that ρ decreases with increasing temperature; thus κ_L decreases further, up to ~15% of κ, with increasing Fe content. In addition, at 300 K, κ_L decreases with increasing Fe content. The mass difference between Fe and Zn scatters phonons (mass fluctuation scattering) and results in a reduction in κ_L with Fe content. This type of scattering is less prominent at elevated temperatures, as shown in Figure 4 where the κ_L values for all specimens are very close to each other above 700 K. Figure 4 also shows that there is no "upturn" in the data at high temperatures, indicative of little or no bipolar contribution to κ in the measured temperature range for all four specimens.

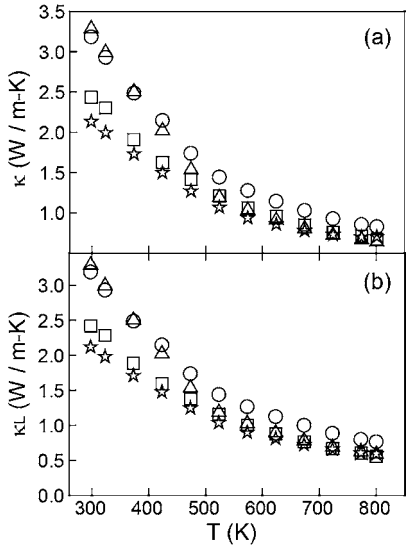

Figure 4. Temperature dependent (a) κ and (b) κ_L for $Cu_2Zn_{1-x}Fe_xSnSe_4$. The symbols corresponding to each specimen are as defined in Figure 3.

The *ZT* values for all specimens were calculated using the measured data in Figures 3 and 4 and are shown in Figure 5. The *ZT* values for all specimens increase rapidly with increasing temperature. A *ZT* value of 0.46 was obtained at 800 K for $Cu_2Zn_{0.4}Fe_{0.6}SnSe_4$. This value is higher than that of $Cu_2ZnSnSe_4$.[10,11] Previous reports show that Cu doping

dx.doi.org/10.1021/ic402455x | Inorg. Chem. 2013, 52, 14364–14367

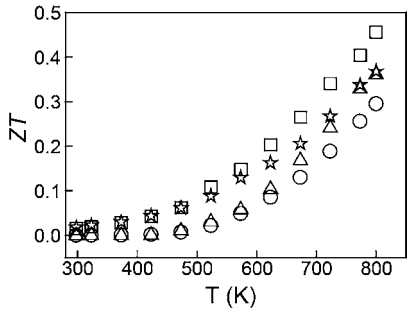

Figure 5. The dimensionless figure of merit, *ZT*, as a function of temperature for $Cu_2Zn_{1-x}Fe_xSnSe_4$. The symbols corresponding to each specimen are as defined in Figure 3.

reduces ρ and κ simultaneously by increasing conduction along the conducting pathways while also increasing local structural disorder, respectively.[9−11] Higher *ZT* values may therefore be possible in these stannite structured compositions by incorporating more Cu.[9−11]

CONCLUSION

$Cu_2Zn_{1-x}Fe_xSnSe_4$ (x = 0.2, 0.4, 0.6, 0.8) solid solutions with the tetragonal stannite structure were prepared by melting, annealing, and hot pressing in order to investigate their crystal structure and high temperature transport properties. Rietveld refinement and elemental analyses confirm the composition of each specimen to be close to that of their nominal compositions. The ρ and κ values decrease significantly with increasing Fe content as compared to $Cu_2ZnSnSe_4$.[10,11] Enhancement of the thermoelectric properties of these *p*-type stannites was therefore achieved by doping with Fe. Further enhancement may be possible at higher Cu concentrations.

ASSOCIATED CONTENT

Supporting Information

Complete X-ray crystallographic CIF files for all compositions. This material is available free of charge via the Internet at http://pubs.acs.org.

AUTHOR INFORMATION

Corresponding Author

*E-mail: gnolas@usf.edu.

Notes

The authors declare no competing financial interest.

ACKNOWLEDGMENTS

Y.D. and G.S.N. gratefully acknowledge financial support from the National Science Foundation and Department of Energy Partnership on Thermoelectric Devices for Vehicle Applications (Grant No. 1048796). H.W. would like to thank the support of the assistant secretary for Energy Efficiency and Renewable Energy of the Department of Energy and the Propulsion Materials program under the Vehicle Technologies program. Oak Ridge National Laboratory is managed by UT-Battelle LLC under contract DE-AC05000OR22725.

REFERENCES

(1) DiSalvo, F. J. *Science* **1999**, *285*, 703−706.
(2) Nolas, G. S.; Sharp, J. W.; Goldsmid, H. J. *Thermoelectrics: Basics Principles and New Materials Developments*; Springer-Verlag: Berlin, 2001.
(3) Tritt, T. M. *Ann. Rev. Mater. Res.* **2011**, *41*, 433−448.
(4) Mahan, G. D. *Solid State Phys.* **1998**, *51*, 81−157.
(5) Plirdpring, T.; Kurosaki, K.; Kosuga, A.; Day, T.; Firdosy, S.; Ravi, V.; Snyder, G. J.; Harnwunggmoung, A.; Sugahara, T.; Ohishi, Y.; Muta, H.; Yamanaka, S. *Adv. Mater.* **2012**, *24*, 3622−3626.
(6) Lu, X.; Morelli, D. T.; Xia, Y.; Zhou, F.; Ozolins, V.; Chi, H.; Zhou, X.; Uher, C. *Adv. Energy Mater.* **2013**, *3*, 342−348.
(7) Lu, X.; Morelli, D. T. *Phys. Chem. Chem. Phys.* **2013**, *15*, 5762−5766.
(8) Dong, Y.; McGuire, M. A.; Yun, H.; DiSalvo, F. J. *J. Solid State Chem.* **2010**, *183*, 606−612.
(9) Liu, M. L.; Chen, I. W.; Huang, F. Q.; Chen, L. D. *Adv. Mater.* **2009**, *21*, 3808−3812.
(10) Shi, X. Y.; Huang, F. Q.; Liu, M. L.; Chen, L. D. *Appl. Phys. Lett.* **2009**, *94*, 122103.
(11) Liu, M. L.; Huang, F. Q.; Chen, L. D.; Chen, I. W. *Appl. Phys. Lett.* **2009**, *94*, 202103.
(12) Zeier, W. G.; Pei, Y.; Pomrehn, G.; Day, T.; Heinz, N.; Heinrich, C. P.; Snyder, G. J.; Tremel, W. *J. Am. Chem. Soc.* **2013**, *135*, 726−732.
(13) Raju, Ch.; Falmbigl, M.; Rogl, P.; Yan, X.; Bauer, E.; Horky, J.; Zehetbauer, M.; Mallik, R. C. *AIP Adv.* **2013**, *3*, 032106.
(14) Liu, H.; Shi, X.; Xu, F.; Zhang, L.; Zhang, W.; Chen, L.; Li, Q.; Uher, C.; Day, T.; Snyder, G. J. *Nat. Mater.* **2012**, *11*, 422−425.
(15) Zhao, L. D.; Berardan, D.; Pei, Y. L.; Byl, C.; Pinsard-Gaudart, L.; Dragoe, N. *Appl. Phys. Lett.* **2010**, *97*, 092118.
(16) Liu, Y.; Zhao, L. D.; Liu, Y.; Lan, J.; Xu, W.; Li, F.; Zhang, B. P.; Berardan, D.; Dragoe, N.; Lin, Y. H.; Nan, C. W.; Li, J. F.; Zhu, H. *J. Am. Chem. Soc.* **2011**, *133*, 20112−20115.
(17) Li, J.; Sui, J.; Pei, Y.; Barreteau, C.; Berardan, D.; Dragoe, N.; Cai, W.; He, J.; Zhao, L. D. *Energy Environ. Sci.* **2012**, *5*, 8543−8547.
(18) Ibáñez, M.; Cadavid, D.; Zamani, R.; García-Castelló, N.; Izquierdo-Roca, V.; Li, W.; Fairbrother, A.; Prades, J. D.; Shavel, A.; Arbiol, J.; Pérez-Rodríguez, A.; Morante, J. R.; Cabot, A. *Chem. Mater.* **2012**, *24*, 562−570.
(19) Ibáñez, M.; Zamani, R.; LaLonde, A.; Cadavid, D.; Li, W.; Shavel, A.; Arbiol, J.; Morante, J. R.; Gorsse, S.; Snyder, G. J.; Cabot, A. *J. Am. Chem. Soc.* **2012**, *134*, 4060−4063.
(20) Zeier, W. G.; LaLonde, A.; Gibbs, Z. M.; Heinrich, C. P.; Panthöfer, M.; Snyder, G. J.; Tremel, W. *J. Am. Chem. Soc.* **2012**, *134*, 7147−7154.
(21) Larson, A. C.; Von Dreele, R. B. *General Structure Analysis System*; Report LAUR 86-748, Los Alamos National Laboratory: Los Alamos, NM, 2004.
(22) Wang, H.; Porter, W. D.; Bottner, H.; Kronig, J.; Chen, L.; Bai, S.; Tritt, T. M.; Mayolet, A.; Senawiratne, J.; Smith, C.; Harris, F.; Gillbert, P.; Sharp, J.; Lo, J.; Kleinke, H.; Kiss, L. *J. Electron. Mater.* **2013**, *42*, 1073−1084.
(23) Olekseyuk, I. D.; Gulay, L. D.; Dydchak, I. V.; Parasyuk, O. V.; Marchuk, O. V. *J. Alloys Compd.* **2002**, *340*, 141−145.
(24) Roque Infante, E.; Delgado, J. M.; López Rivera, S. A. *Mater. Lett.* **1997**, *33*, 67−70.
(25) Schorr, S.; Hoebler, H.-J.; Tovar, M. *Eur. J. Mineral.* **2007**, *19*, 65−73.
(26) Bonazzi, P.; Bindi, L.; Bernardini, G. P.; Menchetti, S. *Can. Mineral.* **2003**, *41*, 639−647.
(27) Sachanyuk, V. P.; Olekseyuk, I. D.; Parasyuk, O. V. *Phys. Status Solidi A* **2006**, *3*, 459−465.
(28) Henao, J. A.; Macías, M. A.; Quintero, M.; Moreno, E.; Morocoima, M.; Quintero, E.; Grima, R.; Tovar, R.; Bocaranda, P. *Chalcogenide Lett.* **2009**, *11*, 583−593.
(29) Goldsmid, H. J.; Sharp, J. W. *J. Electron. Mater.* **1999**, *28*, 869−872.